
Steerable Transformers

Soumyabrata Kundu

Department of Statistics
University of Chicago
Chicago, IL 60637

soumyabratakundu@uchicago.edu

Risi Kondor

Department of Computer Science
Department of Statistics
Computational and Applied Mathematics
University of Chicago
Chicago, IL 60637

risi@cs.uchicago.edu

Abstract

In this work we introduce Steerable Transformers, an extension of the Vision Transformer mechanism that maintains equivariance to the special Euclidean group $SE(d)$. We propose an equivariant attention mechanism that operates on features extracted by steerable convolutions. Operating in Fourier space, our network utilizes Fourier space non-linearities. Our experiments in both two and three dimensions show that adding a steerable transformer encoder layer to a steerable convolution network enhances performance.

1 Introduction

Transformers have emerged as the preferred architecture for natural language processing tasks, with recent powerful models like Chat-GPT employing this framework. Their relatively straightforward design, coupled with their remarkable success, has led to their widespread adoption across various domains, including image classification [11], object detection [5], and graph-based problems [12]. The self-attention mechanism [2] employed in transformer architectures has proven to be crucial for capturing relationships between different parts of input sequences. Dosovitskiy et al. [11] introduced transformers as an alternative to traditional convolutional architectures for image classification tasks. Unlike convolutional neural networks (CNNs), which focus on local neighborhoods, transformers excel at capturing relations across different parts of the input, including in images.

Equivariant neural network architectures have gained significant popularity in recent years due to their inherent ability to comprehend the underlying symmetries of problems, making them highly effective tools for real-world scenarios characterized by such symmetries. For instance, achieving equivariance to the permutation group S_n is crucial in graph-based problems, where the structure of the graph remains invariant under permutations. Similarly, in image-related tasks, it is desirable to have equivariance to rigid body transformations such as rotations and translations. Recent studies have demonstrated the remarkable efficacy of these equivariant architectures in addressing such challenges without relying on brute-force techniques like data augmentation [40, 20].

In image classification tasks, steerable convolutions have proven to be a powerful tool for achieving equivariance to the group $SE(d)$, which encompasses rotations and translations in d dimensions [40, 10, 37]. Steerable convolution networks primarily operate in Fourier space, leveraging representations of the underlying group to encode rotation and translation equivariant features from the data [9, 8, 37]. Nevertheless, these architectures, rooted in convolutions, retain the ability to learn local neighborhoods. Conversely, transformer architectures excel in learning relationships between different regions of an image. Our contribution lies in integrating these two concepts—vision transformers and steerable convolutions—yielding steerable transformers capable of effectively capturing both local and global patterns in images.

In this paper we introduce a novel steerable transformer architecture for image recognition. The architecture draws inspiration mainly from the works of Dosovitskiy et al. [11] and Fuchs et al. [13]. Dosovitskiy et al. [11] pioneered the use of transformers in vision tasks by segmenting images into sequences. They also introduced a hybrid approach, incorporating learned features from CNN layers instead of directly inputting images into transformers. On the other hand, Fuchs et al. [13] introduced an attention-based architecture for processing 3D point cloud data, integrating the self-attention mechanism into Tensor Field Networks [32]. Similar to steerable CNNs [9] and Tensor Field Networks [32], steerable transformers operate in Fourier space, leveraging representations of the underlying symmetry group to learn equivariant features. The self-attention mechanism in steerable transformers is designed akin to that in [13]. Similar to [33], we use this kind of architecture in addition with steerable convolutions[40, 37]. Other transformer based equivariant architecture like [42, 27] base their design on [24], where they have completely replaced the convolution architecture for an attention based mechanism. Both Dosovitskiy et al. [11] and Fuchs et al. [13] employ learnable positional encodings. While the seminal work by Vaswani et al. [33] utilizes predefined functions for positional encoding, our approach combines both strategies by multiplying a fixed function with a learnable scalar. Unlike [42, 27], who employ invariant positional encoding, we use equivariant positional encoding.

2 Related Work

The original idea of attention was introduced by Bahdanau et al. [2], for sequence modeling. Vaswani et al. [33] introduced the transformer encoder-decoder architecture for translation tasks in natural language processing. Dosovitskiy et al. [11] proposed the transformer architecture for vision tasks. However these transformer architectures are not linear in their inputs and hence break the equivariance structure of traditional CNN. Since then there has been a flurry of papers trying to make these structures equivariant. While [11] advocated for a hybrid architecture where the features are extracted from traditional CNN. Ramachandran et al. [24] introduced a stand alone attention based architecture which completely replaces traditional CNNs.

Shaw et al. [29] proposed learnable relative positional encoding instead of absolute positional encoding in the original work [33], to encode the relative positions of input sequences. Romero et al. [27] showed that vision transformers [11] with relative positional encoding is translation equivariant. They extended the idea of [24] to incorporate rotation and translation equivariance in the 2D regime, by lifting the attention mechanism to be defined on the group $SE(2)$. For this they proposed a positional encoding operator and use regular representations of the group instead of irreducible representations. Xu et al. [42] introduces a novel positional encoding in the method proposed in [27] to enhance its performance. Romero et al. [26] incorporated attention in convolution itself by defining attention score on the equivariance groups.

In the 3D regime there have been efforts to use attention in vision task, however to the best of our knowledge, only on point cloud data and not volumetric data. Fuchs et al. [13] proposed an $SE(3)$ equivariant architecture for point cloud data by adding self-attention mechanism to the rotation, translation and permutation equivariant Tensor Field network [32]. Chen et al. [7] achieved equivariance in attention mechanisms by mapping the data onto $SE(3)$ equivariant and invariant features. These maps are based on the work of Villar et al. [34]. Hutchinson et al. citephutchinson2021lietransformer introduced an attention mechanism that is equivariant to the action of Lie groups using regular representations of the group and built a transformer architecture based on that. Chatzipantazis et al. [6] introduced $SE(3)$ equivariant attention for shape reconstruction tasks.

3 Background

In this section we introduce the relevant background required to design the steerable transformer architecture.

3.1 The Multihead Self-Attention Mechanism

The attention mechanism, initially introduced by Bahdanau et al. [2] for sequence-to-sequence tasks, involves three main components: query vectors q_i , key vectors k_i , and value vectors v_i for each input in a sequence. These vectors are utilized to compute attention weights, denoted α_{ij} , which determine

the relevance of each input vector in producing the output. The score function $s(q_i, k_j)$ calculates the compatibility between query and key vectors. The softmax of these scores yields the attention weights α_{ij} . Finally, we get the output by linearly combining α_{ij} with the value vectors v_i :

$$\text{ATTN}(q_i, \{k_i\}, \{v_i\}) = \sum_{j=1}^N \alpha_{ij} v_j, \quad \alpha_{ij} = \frac{\exp(s(q_i, k_j))}{\sum_{j=1}^N \exp(s(q_i, k_j))}.$$

The score function $s(q_i, k_j)$ in the scaled dot-product attention mechanism [33], for a fixed i , is calculated as:

$$s(q_i, k_j) = \frac{q_i^T k_j}{\sqrt{d_K}}.$$

Vaswani et al. [33] proposed a Multihead version of this attention mechanism which involves stacking multiple attention mechanisms, concatenating their outputs and applying a linear transformation to get the final result:

$$\text{MULTI-ATTN}(q_i, \{k_i\}, \{v_i\}) = \text{Concat}(\text{ATTN}^1, \dots, \text{ATTN}^h)W_O,$$

where $W_O \in \mathbb{R}^{h d_V \times d_{\text{model}}}$. Here d_{model} is the dimension of the output which is same as the dimension of the input vectors. This dimension is fixed through the Transformer encoder structure. Typically, the query, key, and value vectors are obtained through learnable linear embedding followed by adding *positional encoding*.

Positional Encoding: Positional encoding in transformers is a technique employed to incorporate positional information about words or tokens into the input embeddings of a sequence. In vision tasks, these encodings inform the network about the original locations of different portions of the image. In the seminal work by Vaswani et al. [33], they utilized sine and cosine functions of varying frequencies for positional encoding. Relative positional encoding, introduced by Shaw et al. [29], represents an extension or variation of traditional positional encoding. Its goal is to use learnable position encoding that capture the relative distances between input sequences. As we explain below, relative positional encoding is crucial for achieving equivariance.

3.2 Vision Transformers

Dosovitskiy et al. [11] extended the use of the transformer architecture to vision tasks. In their approach, they divided the image into equal-sized portions and fed them into the encoder part of the transformer architecture. They utilize the features obtained from the encoder for classification. Assuming a single input channel, the vision transformer layer can be summarized as follows:

$$\begin{aligned} z_0 &= [\mathbf{x}_1 E, \mathbf{x}_2 E, \dots, \mathbf{x}_N E] + E_{\text{pos}} & E \in \mathbb{R}^{p \times d_{\text{model}}}, \quad E_{\text{pos}} \in \mathbb{R}^{N \times d_{\text{model}}} \\ z'_\ell &= \text{MULTI-ATTN}(\text{LN}(z_{\ell-1})) + z_{\ell-1} & \ell = 0, 1, \dots, L \\ z'_\ell &= \text{MLP}(\text{LN}(z_{\ell-1})) + z'_\ell & \ell = 0, 1, \dots, L. \end{aligned}$$

Here, $\mathbf{x}_i \in \mathbb{R}^p$ represents a portion of the image which serves as the input, E is the learnable linear embedding matrix, and E_{pos} is the positional encoding. LN denotes a normalization layer, and MLP stands for a multilayer perceptron. d_{model} is the dimension of the embedding fed into the transformer, which remains fixed throughout the entire encoder layer. Typically, the MLP layer comprises two hidden layers separated by a non-linearity [33, 11].

3.3 Equivariance

Equivariance refers to a property where a mapping between vector spaces preserves the action of a group G . For each $g \in G$, a linear map $T_g : \mathcal{V} \rightarrow \mathcal{V}$ is defined on a vector space \mathcal{V} . Given actions T_g and T'_g on vector spaces \mathcal{V} and \mathcal{W} respectively, a map $\phi : \mathcal{V} \rightarrow \mathcal{W}$ is considered equivariant if:

$$\phi(T_g(\mathbf{v})) = T'_g(\phi(\mathbf{v})) \quad \mathbf{v} \in \mathcal{V}.$$

Equivariance naturally emerges as a constraint in various real-world scenarios. For instance, in Graph Neural Networks, equivariance to the permutation group S_n is fundamental [31, 35]. Similarly, in vision tasks, equivariance to rotation and reflection symmetries, i.e., the action of the Euclidean group, is desirable. There is now an extensive literature on equivariant neural networks, in particular, focusing on cases where ϕ is linear [40, 10, 37, 9, 8, 36, 16, 1].

3.4 Steerable Neural Networks

Steerable Networks are engineered to exhibit equivariance to the special Euclidean group $\text{SE}(d)$ in d dimensions. Consider an d -dimensional image with a single input channel, represented by the function $f^{\text{in}} : \mathbb{R}^d \rightarrow \mathbb{R}$, which has compact support. These networks employ steerable convolution layers, which can be expressed as convolutions on the group $\text{SE}(d)$ [37, 36]:

$$f^{\text{out}}(\mathbf{x}, R) = \int_{\text{SO}(d)} \int_{\mathbb{R}} f^{\text{in}}(\mathbf{x} + R\mathbf{y}) w(\mathbf{y}) d\mathbf{y} d\mu(R), \quad (1)$$

$$f^{\text{out}}(\mathbf{x}, R) = \int_{\text{SO}(d)} \int_{\mathbb{R}} f^{\text{in}}(\mathbf{x} + R\mathbf{y}, RR') w(\mathbf{y}, R') d\mathbf{y} d\mu(R'). \quad (2)$$

Here μ denotes the Haar measure on $\text{SO}(d)$. Equation (1) represents the formula for the first layer, while (2) represents subsequent layers. The presence of two distinct formulas is due to the fact that the input to the first layer is a vector field on \mathbb{R}^d , whereas the input to subsequent layers is a vector field on $\text{SE}(d)$. These linear mappings possess a key property: whenever the input map f^{in} undergoes a transformation by an element in $\text{SE}(d)$, the resulting output f^{out} also undergoes the same transformation. This property means that if under the action of the group f^{in} changes to

$$f^{\text{in}'}(\mathbf{x}) = (t, R) \cdot f^{\text{in}}(\mathbf{x}) = f^{\text{in}}(R\mathbf{x} + t) \quad (3)$$

then f^{out} changes to

$$f^{\text{out}'}(\mathbf{x}, R') = (t, R) \cdot f^{\text{out}}(\mathbf{x}, R') = f^{\text{out}}(R\mathbf{x} + t, RR'). \quad (4)$$

For compact groups like $\text{SO}(d)$, where discretization is not straightforward, it is advantageous to compute the rotation component of the output feature map of (2) in Fourier space [40]. Leveraging the convolution theorem, equation (2) in Fourier space becomes a product of the Fourier transforms of the input and the weights. The Fourier transform of a function f on a compact group can be computed by integrating it against its irreducible representations or *irreps* (see Appendix for definition):

$$\widehat{f}(\rho) = \int_{\text{SO}(d)} f(R) \rho(R) d\mu(R).$$

These Fourier space vector fields possess the property that under input transformations like (3), the output transforms to $\rho(R) \widehat{f^{\text{out}}}(\mathbf{R}\mathbf{x} + t, \rho)$ [9, 37].

In the 2D case, the irreps of $\text{SO}(2)$ are just complex exponential indexed by integers, $\rho_k(\theta) = e^{ik\theta}$. Therefore, the k 'th frequency component of the output feature map is a function $\widehat{f_k^{\text{out}}} : \mathbb{R}^2 \rightarrow \mathbb{C}$. For the 3D case, the irreps of $\text{SO}(3)$ are indexed by integers $\ell \geq 0$, represented by $\rho_\ell(R) = D^\ell(R)$, known as the Wigner matrices [38], which are unitary matrices of dimension $2\ell + 1$. Correspondingly, the ℓ 'th Fourier component of the output feature map is a function $\widehat{f_\ell^{\text{out}}} : \mathbb{R}^3 \rightarrow \mathbb{C}^{2\ell+1}$.

Non-linearities: In steerable neural networks, utilizing non-linearities like ReLU in Fourier space can disrupt equivariance. One approach to mitigate this issue is to transition back to real space, apply the desired non-linearity there, and then return to Fourier space. This method, for instance, is employed in [10]. However, this back-and-forth transformation between real and Fourier space can be computationally expensive and error-prone, especially on groups like $\text{SO}(3)$ where the grid is non-uniform.

As an alternative, Fourier space non-linearities are preferred in steerable neural networks. These non-linearities act directly on Fourier space while preserving equivariance. Several such non-linearities can be found in the literature. For instance, Worall et al. [40] apply non-linearity to the norm of the Fourier vector, as the norm remains invariant under rotations. Other works such as [16, 1] utilize the Clebsch–Gordan non-linearity, which involves a tensor product of Fourier vectors followed by a Clebsch–Gordan decomposition. Weiler et al. [37] introduce another steerable convolution filter to serve as a non-linearity. These methods enable effective non-linear transformations in Fourier space while maintaining equivariance.

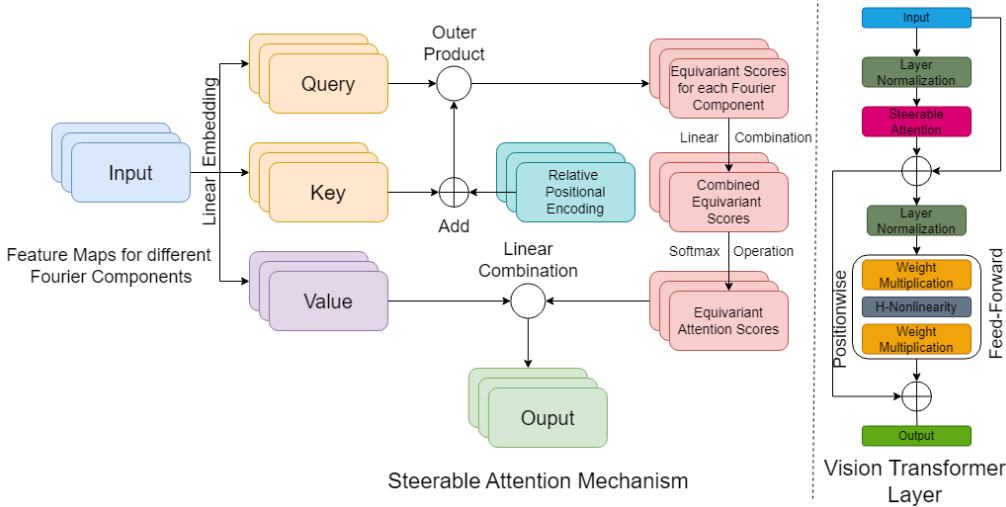


Figure 1: The schematic illustrates the steerable attention mechanism (left) and a steerable transformer encoder layer (right); c.f. Figure 1 in [11]). The steerable attention mechanism is shown for a single head ($h = 1$) and one query dimension ($d_K = 1$). The stacks of feature maps represent different Fourier components, and the H -Nonlinearity denotes the harmonic non-linearity described in [40].

4 Method

The methodology behind steerable transformers builds on the foundation established by vision transformers [11], which rely on linear embeddings of fixed-size image patches along with positional encoding for these patches. A hybrid architecture discussed in the same work integrates features maps produced by CNNs as input to the transformer encoder. In the case of steerable transformers, we adopt this hybrid approach, with feature maps generated by steerable convolution layers serving as input to the transformer encoder.

In Section 3.4, we discussed that the output of steerable networks is a compactly supported function on a continuous domain. However, practical neural networks operate on finite resolution rasterized images. Consequently, in real-world implementations, the output features for a particular irrep are represented as a collection of complex vectors on a grid. For simplicity, let us assume that there are N such grid points. For C channels, the input sequence to the transformer is described by:

$$f^{\text{in}}(\mathbf{x}_i, \rho) \in \mathbb{C}^{d_\rho \times C}, \quad i = 1, 2, \dots, N, \quad k \in \mathbb{Z}. \quad (5)$$

In two dimensions, d_ρ is always 1, while in three dimensions, the ℓ^{th} component has $d_\rho = 2\ell + 1$.

4.1 Positional Encoding

Before we delve into the steerable version of self-attention, let us first explore a steerable approach to positional encoding. In the seminal work by Vaswani et al. [33], sine and cosine functions of varying frequencies were utilized to encode positions. In contrast, Dosovitskiy et al. [11] employed learnable positional embeddings for vision transformers. In our approach, we adopt a hybrid method, by having both learnable and fixed components in positional encoding.

Relative positional encoding, introduced by Shaw et al. [29], considers positional encoding as learned functions of the relative distances between input sequences. Romero et al. [27] demonstrated that self-attention mechanisms with relative positional encoding exhibit translation equivariance. Therefore, the positional embeddings we seek are functions $P_{ij}^\rho = P(\mathbf{x}_i - \mathbf{x}_j, \rho)$, inherently invariant to translations.

To introduce the notion of steerability, we aim for P_{ij}^ρ to transform as $\rho(R)P_{ij}^\rho$ whenever the grid locations \mathbf{x}_i undergo a rotation R . Essentially we will be using the Fourier basis to enforce the equivariance (3), (4). In two dimensions, this boils down to:

$$P(\mathbf{x}, k) = \phi(r, k)e^{-ik\theta}, \quad \mathbf{x} = [r \cos \theta, r \sin \theta]^T, \quad k \in \mathbb{Z}. \quad (6)$$

Here, $\phi(r, k)$ modulates the encoding strength for nearby and distant points. In the 3D case, we have

$$P(\mathbf{x}, \ell) = \phi(r, l) Y^\ell(\theta, \phi), \quad \mathbf{x} = [r \sin \theta \cos \phi, r \sin \theta \sin \phi, r \cos \theta]^T, \quad \ell \in \mathbb{Z}_{\geq 0}, \quad (7)$$

where Y^ℓ denotes the spherical harmonics [4]. The steerability property of positional encoding implies $P_{ii}^\rho = 0$ for any ρ except for the constant representation, i.e., $k = 0$ and $\ell = 0$ in two and three dimensions, respectively (as $P_{ii}^\rho = \rho(R)P_{ii}^\rho$ for any R). This condition can be enforced by setting ϕ to zero when $r = 0$. For our experiments, we employed $\phi(r, \rho) = w_\rho e^{-r^2} \mathbb{1}_{r>0}$, where w_ρ is a learnable scalar. This kind of exponential modulation of the radial component is also seen in [40, 37], and the resulting positional encoding assigns higher weight to neighboring points, and the weights decrease as points move further apart. In our actual implementation, we have different learnable scalars not only for different Fourier components but also for different heads and query dimensions.

4.2 Steerable Self-Attention Mechanism

The query, key, and value embeddings are obtained by multiplying the input f^{in} in (5) with learnable weight matrices. Additionally, positional encoding is incorporated into the key embeddings [29].

$$\begin{aligned} \mathbf{q}_i^\rho &= f^{\text{in}}(\mathbf{x}_i, \rho) \mathbf{W}_Q^\rho & \mathbf{W}_Q^\rho &\in \mathbb{C}^{d_{\text{model}} \times d_K} \\ \mathbf{k}_{ij}^\rho &= f^{\text{in}}(\mathbf{x}_i, \rho) \mathbf{W}_K^\rho + P(\mathbf{x}_i - \mathbf{x}_j, \rho) & \mathbf{W}_K^\rho &\in \mathbb{C}^{d_{\text{model}} \times d_K} \\ \mathbf{v}_i^\rho &= f^{\text{in}}(\mathbf{x}_i, \rho) \mathbf{W}_V^\rho & \mathbf{W}_V^\rho &\in \mathbb{C}^{d_{\text{model}} \times d_V} \end{aligned}$$

Next, the score function for each Fourier component is calculated by taking the dot product between the query and key embeddings. The individual scores from each Fourier component can be mixed together using scalar weights. The attention scores are obtained by applying the softmax function to the raw scores. Since we are dealing with complex numbers, we use the absolute value of these scores:

$$s(\mathbf{q}_j^\rho, \mathbf{k}_{ij}^\rho) = \frac{\text{vec}(\mathbf{q}_j^\rho)^\dagger \text{vec}(\mathbf{k}_{ij}^\rho)}{\sqrt{d_K}} \quad s_{ij}^\rho = \sum_{\rho'} w_{\rho\rho'}^{(1)} s_{ij}^{\rho'} \quad \alpha_{ij}^\rho = \frac{\exp(|s_{ij}^\rho|)}{\sum_{j'=1}^N |s_{ij'}^\rho|}$$

Here, the vec operation flattens the matrix into a vector. Since the vectors are complex-valued, the dot product involves the conjugate transpose, denoted by \cdot^\dagger , instead of a regular transpose. Finally, the output for each position and Fourier component is computed as a weighted sum of the value vectors using the attention scores, and then combined again using scalar weights:

$$f^{\text{out}}(\mathbf{x}_i, \rho) = \sum_{\rho'} \sum_{j=1}^N w_{\rho\rho'}^{(2)} \alpha_{ij}^{\rho'} \mathbf{v}_j^\rho.$$

The scalar weights $w_{\rho\rho'}^{(1)}, w_{\rho\rho'}^{(2)} \in \mathbb{C}$ can be fixed, learnable, or a combination of both, offering a variety of models to work with. This self-attention mechanism maintains equivariance, as demonstrated by the following proposition.

Proposition 1. *If the input to a steerable transformer self-attention layer transforms as $f^{\text{in}}(\mathbf{x}_i, \rho) \mapsto \rho(R) f^{\text{in}}(R\mathbf{x}_i + \mathbf{t}, \rho)$, then the output also transforms as $f^{\text{out}}(\mathbf{x}_i, \rho) \mapsto \rho(R) f^{\text{out}}(R\mathbf{x}_i + \mathbf{t}, \rho)$.*

Despite the softmax operation's lack of equivariance, in this scenario, the dot product structure of the score function maintains rotational invariance, thereby preserving equivariance. For multihead attention, this mechanism is repeated independently for h heads. Finally, the outputs are concatenated, and each Fourier component is scaled by another matrix $\mathbf{W}_O^\rho \in \mathbb{C}^{h d_V \times d_{\text{model}}}$. Consistent with [33], we choose $d_V = d_K = d_{\text{model}}/h$.

4.3 Position-wise Feed Forward Layer

In a transformer architecture, the self-attention layer is typically followed by a multilayer perceptron (MLP) layer. This MLP layer commonly consists of two linear layers separated by a non-linearity [33]. The linear layers themselves do not affect equivariance as they are applied to the input from the right:

$$f^{\text{out}}(\mathbf{x}_i, \rho) = \sigma(f^{\text{in}}(\mathbf{x}_i, \rho) W_1) W_2 \quad \text{where} \quad W_1, W_2^T \in \mathbb{C}^{d_{\text{model}} \times d_{\text{hidden}}}.$$

Datasets	Model	Frequency Cutoff	Accuracy	Parameter ($\sim \times 10^6$)
Rotated MNIST	Steerable Convolution	$k = 4$	98.72 ± 0.02	1.98
		$k = 8$	98.97 ± 0.01	3.94
	Steerable Convolution (Without Transformer)	$k = 4$	98.70 ± 0.05	0.46
		$k = 8$	98.97 ± 0.05	0.92
	Steerable Transformer	$k = 4$	98.82 ± 0.04	1.13
		$k = 8$	99.03 ± 0.04	2.24
ModelNet10 (z Rotation) (SO(3) Rotation)	Steerable Convolution	$\ell = 4$	90.13 ± 0.52	1.08
			86.62 ± 0.25	
	Steerable Convolution (Without Transformer)	$\ell = 4$	89.51 ± 0.55	0.48
			86.58 ± 0.92	
	Steerable Transformer	$\ell = 4$	90.40 ± 0.25	0.92
			86.80 ± 0.58	

Table 1: Comparison of steerable transformers and steerable convolutions. For each dataset, the first row features an architecture with only steerable convolutions and an increased number of channels to match the parameter count of the steerable transformers. The second row presents the same architecture as the steerable transformer but without the transformer encoder layer. The third row displays the steerable transformer architecture. The radial resolution was fixed for these experiments. A more detailed comparison is available in the Appendix Table 4. The mean and sd are reported for 5 runs. For ModelNet10 we have reported both the z rotation and SO(3) rotation variations.

Here, d_{hidden} represents the hidden dimension between the two linear layers. However, when it comes to the non-linearity, caution is needed. As discussed in Section 3.4, typical non-linearities like ReLU or softmax may break equivariance. Instead, we require a Fourier space non-linearity. For our experiments, we utilize a non-linearity proposed by Worrall et al. [40], where they apply ReLU to the magnitude of the equivariant vectors:

$$\sigma(f(\mathbf{x}, \rho)) = \frac{\text{ReLU}(\|f(\mathbf{x}, \rho)\| + b)}{\|f(\mathbf{x}, \rho)\|} f(\mathbf{x}, \rho).$$

Here, b is a learnable weight. Since the norm of the features in Fourier space is invariant to rotations, this non-linearity preserves equivariance. Following the convention in [33], we set $d_{\text{hidden}} = 2d_{\text{model}}$.

4.4 Layer Normalization

Another crucial component of the transformer architecture is layer normalization. Notably, the norm of equivariant vectors remains invariant under the Fourier transform, as it preserves the \mathcal{L}_2 norm. Leveraging this property, we can derive a steerable normalization as follows:

$$\text{LN}(f)(\mathbf{x}, \rho) = \frac{f(\mathbf{x}, \rho)}{\sum_{\rho} \|f(\mathbf{x}, \rho)\|^2}.$$

Indeed, the sum over ρ theoretically extends over all irreps of the group, but in practical implementations, it is truncated at particular values, which serves as a hyperparameter that can be tuned. This type of normalization was employed in the 2D context by Worrall et al. [40].

5 Experiments

We evaluate the performance of our steerable transformer architecture in both two and three dimensions. For all experiments, we used a hybrid architecture combining steerable convolutions and steerable transformer encoder layers, trained using the Adam Optimizer [15]. The architecture consists of steerable CNN blocks and a steerable transformer encoder. Each steerable convolution block includes two steerable convolutions separated by a Clebsch–Gordan nonlinearity [1, 16] and followed by layer normalization, as detailed in Section 4.4. After a convolution block, a transformer encoder is applied. This pattern is repeated twice, followed by a final convolution block with a kernel size equal to the input size, downsampling the image to one pixel per Fourier component and channel.

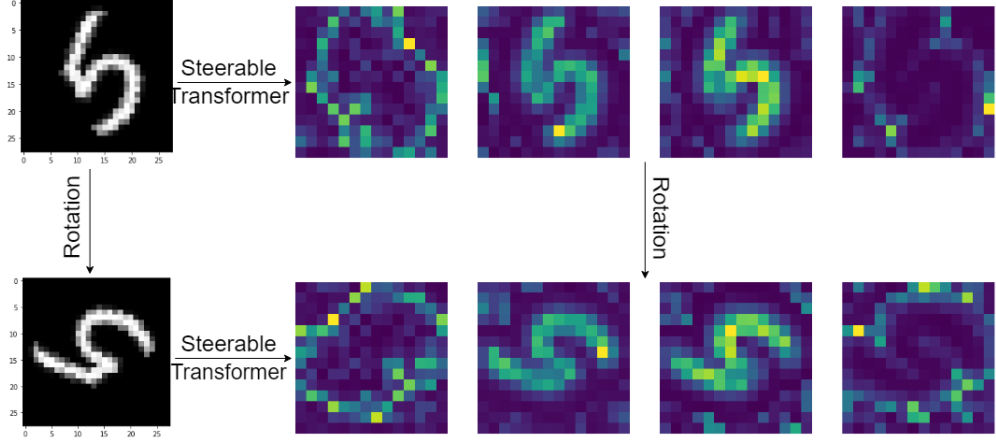


Figure 2: The figure demonstrates the equivariance of attention scores in a trained steerable transformer. For a fixed pixel i , we have plotted the maximum attention score for that pixel ($\max_j \alpha_{ij}$). The different subfigures represent individual heads. The first and last heads appear to capture the object’s boundary, while the other two heads focus on the object’s body.

This step is followed by taking the norm, ensuring rotational and translational invariance due to the properties of the Fourier transform. The final convolution is followed by two fully connected layers with a ReLU activation and a dropout layer, using a dropout probability of 0.7 as in [20].

We present results for two datasets: Rotated MNIST (2D) and ModelNet10 (3D). Table 1 provides a detailed comparison of the steerable architecture with and without transformers. Results are reported for three configurations: one with steerable transformers, one with the same architecture minus the transformer encoder layers, and another with steerable convolutions but with additional channels to match the parameter count of the steerable transformers.

5.1 Rotated MNIST

Rotated MNIST, a variant of the original MNIST dataset [17], consists of images subjected to random rotations and includes 12,000 training images and 50,000 testing images. Details on the architecture and training can be found in the Appendix.

Table 1 compares the performance of steerable transformers and steerable convolutions. It clearly demonstrates that adding a transformer encoder to steerable convolutions improves performance, even with a low Fourier cutoff. Simply increasing the number of parameters in convolutions by adding more channels does not improve performance and likely results in overfitting. Table 2 presents a comparison of steerable transformers with other attention-based methods reported for this dataset. Our approach shows significantly superior performance compared to the others.

5.2 ModelNet10

ModelNet10 [41] is a dataset comprising 3D CAD models representing 10 common object categories with a train:test split of 3991:908. Each category contains a collection of triangular meshes representing objects in various orientations and scales, facilitating the training and evaluation of algorithms for 3D object recognition and classification tasks. With a predefined split into training and testing sets, ModelNet10 serves as a benchmark dataset for assessing the generalization performance of algorithms. For the experiments, 2,048 points from the shape surface are uniformly sampled using the farthest point sampling algorithm. The point cloud data was then embedded in a grid to get voxel data (see Figure 3 in Appendix). Additionally, we considered two kinds of perturbations of this dataset : the images are perturbed by a random rotation along the "gravity up" direction (z rotation)

Method	error%
α -R4 CNN[26]	1.69
GSA-Nets[27]	2.03
GE-ViT[42]	1.99
Our ($k = 4$)	1.18
Our ($k = 8$)	0.97

Table 2: Comparison of the performance of the equivariant attentive architecture on the Rotated MNIST dataset.

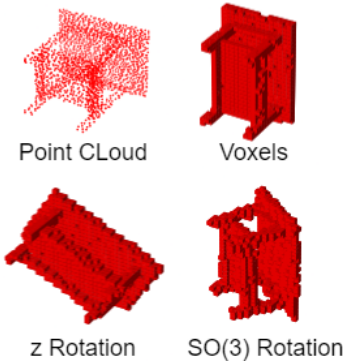


Figure 3: Examples from the ModelNet10 dataset are shown in various formats: point cloud, voxel representation, and rotated perturbations of voxels.

	Method	Accuracy	Parameters ($\sim \times 10^6$)
Point Cloud	ECC [30]	90.8	-
	SO-Net [18]	93.9	2.5
	Rot-SO-Net [19]	94.5	2.5
Voxel	3D ShapeNets[41]	83.5	12
	VRN [3]	91.3	18
	VoxNet [21]	92.0	0.92
	FusionNet [14]	93.1	120
	ORION [28]	93.8	0.91
	Cubenet [39]	94.6	4.5
	Our	91.1	0.92

Table 3: Comparison of performance on ModelNet10 with z rotation perturbation. Other methods used both train and test time augmentation, while we applied augmentation only during test time, not during training.

and also random rotations from $SO(3)$. We also rescale the voxel values to $[-1, 5]$ instead of $[0, 1]$ as in [3], who showed it helps with sparse voxel volumes. The details of architecture and training are provided in the Appendix.

Table 1 shows the comparison of the steerable transformer architecture with steerable convolutions for a frequency cutoff of $\ell = 4$. The results indicate a significant improvement due to the introduction of the steerable transformer encoder layer across both variations of the dataset. Table 3 presents a comparison with other methods (not attention-based) on the z -rotated version of the dataset. Unlike our approach, which does not use train-time augmentation, all other methods are trained with augmentation involving 12 uniformly stratified rotations along the z -axis. For a fair comparison, we applied test-time augmentation by averaging the accuracy of all 12 predictions for each test data point. Despite not using train-time augmentation and having fewer parameters, our method achieves performance comparable to the other methods.

6 Limitations

The use of transformer architecture comes with its challenges. For instance, the dot product structure used in attention scores can create a memory bottleneck for large images, restricting the network size and batch size during training. Scaling up these architectures is essential to fully understand the benefits of the attention mechanism in improving performance. Our experiments on Rotated MNIST and ModelNet10 were conducted with relatively small Fourier cutoffs ($k = 8$ for Rotated MNIST and $\ell = 4$ for ModelNet10). We believe that using higher values for these Fourier cutoffs would enhance performance, but implementing them in a steerable transformer architecture would necessitate scaling up to accommodate larger models.

7 Conclusions

The transformer framework is increasingly being adopted across various machine learning fields, including computer vision, due to its exceptional ability to capture relationships across different parts of the input. In this work, we introduce steerable transformer encoders that can be used in conjunction with steerable convolutions. While convolutions excel at capturing local relationships, incorporating the attention mechanism, which captures global relationships, enhances performance, as demonstrated in our experiments. We believe that this architecture has the potential to make a significant impact in fields such as medical imaging, where equivariance is critical.

References

- [1] B. Anderson, T. S. Hy, and R. Kondor. Cormorant: Covariant molecular neural networks. *Advances in neural information processing systems*, 32, 2019.
- [2] D. Bahdanau, K. Cho, and Y. Bengio. Neural machine translation by jointly learning to align and translate. *CoRR*, abs/1409.0473, 2014. URL <https://api.semanticscholar.org/CorpusID:11212020>.
- [3] A. Brock, T. Lim, J. M. Ritchie, and N. Weston. Generative and discriminative voxel modeling with convolutional neural networks. *ArXiv*, abs/1608.04236, 2016. URL <https://api.semanticscholar.org/CorpusID:2271164>.
- [4] W. E. Byerly. *An elemenatary treatise on Fourier's series, and spherical, cylindrical, and ellipsoidal harmonics, with applications to problems in mathematical physics*. Dover Publications, 1893.
- [5] N. Carion, F. Massa, G. Synnaeve, N. Usunier, A. Kirillov, and S. Zagoruyko. End-to-end object detection with transformers. In *European conference on computer vision*, pages 213–229. Springer, 2020.
- [6] E. Chatzipantazis, S. Pertigkiozoglou, E. Dobriban, and K. Daniilidis. Se (3)-equivariant attention networks for shape reconstruction in function space. *arXiv preprint arXiv:2204.02394*, 2022.
- [7] N. Chen and S. Villar. Se (3)-equivariant self-attention via invariant features. In *Machine Learning for Physics NeurIPS Workshop*, 2022.
- [8] T. Cohen and M. Welling. Group equivariant convolutional networks. In *International conference on machine learning*, pages 2990–2999. PMLR, 2016.
- [9] T. S. Cohen and M. Welling. Steerable CNNs. In *International Conference on Learning Representations*, 2017. URL <https://openreview.net/forum?id=rJQKYt511>.
- [10] T. S. Cohen, M. Geiger, J. Koehler, and M. Welling. Spherical CNNs. In *International Conference on Learning Representations*, 2018.
- [11] A. Dosovitskiy, L. Beyer, A. Kolesnikov, D. Weissenborn, X. Zhai, T. Unterthiner, M. Dehghani, M. Minderer, G. Heigold, S. Gelly, J. Uszkoreit, and N. Houlsby. An image is worth 16x16 words: Transformers for image recognition at scale. *ArXiv*, abs/2010.11929, 2020. URL <https://api.semanticscholar.org/CorpusID:225039882>.
- [12] V. P. Dwivedi and X. Bresson. A generalization of transformer networks to graphs. *arXiv preprint arXiv:2012.09699*, 2020.
- [13] F. Fuchs, D. Worrall, V. Fischer, and M. Welling. Se (3)-transformers: 3d roto-translation equivariant attention networks. *Advances in neural information processing systems*, 33:1970–1981, 2020.
- [14] V. Hegde and R. Zadeh. Fusionnet: 3d object classification using multiple data representations. *arXiv preprint arXiv:1607.05695*, 2016.
- [15] D. P. Kingma and J. Ba. Adam: A method for stochastic optimization. *CoRR*, abs/1412.6980, 2014. URL <https://api.semanticscholar.org/CorpusID:6628106>.
- [16] R. Kondor, Z. Lin, and S. Trivedi. Clebsch–gordan nets: a fully fourier space spherical convolutional neural network. In S. Bengio, H. Wallach, H. Larochelle, K. Grauman, N. Cesa-Bianchi, and R. Garnett, editors, *Advances in Neural Information Processing Systems 31*, pages 10117–10126. Curran Associates, Inc., 2018.
- [17] Y. LeCun and C. Cortes. The mnist database of handwritten digits. 2005. URL <https://api.semanticscholar.org/CorpusID:60282629>.

[18] J. Li, B. M. Chen, and G. H. Lee. So-net: Self-organizing network for point cloud analysis. In *2018 IEEE/CVF Conference on Computer Vision and Pattern Recognition*, pages 9397–9406, 2018. doi: 10.1109/CVPR.2018.00979.

[19] J. Li, Y. Bi, and G. H. Lee. Discrete rotation equivariance for point cloud recognition. In *2019 International conference on robotics and automation (ICRA)*, pages 7269–7275. IEEE, 2019.

[20] D. Marcos, M. Volpi, N. Komodakis, and D. Tuia. Rotation equivariant vector field networks. In *Proceedings of the IEEE International Conference on Computer Vision*, pages 5048–5057, 2017.

[21] D. Maturana and S. Scherer. Voxnet: A 3d convolutional neural network for real-time object recognition. In *2015 IEEE/RSJ International Conference on Intelligent Robots and Systems (IROS)*, pages 922–928, 2015. doi: 10.1109/IROS.2015.7353481.

[22] J. Munkres. *Topology; a First Course*. Prentice-Hall, 1974. ISBN 9780139254956. URL <https://books.google.com/books?id=LtEPQAQAMAAJ>.

[23] F. Peter and H. Weyl. Die vollständigkeit der primitiven darstellungen einer geschlossenen kontinuierlichen gruppe. *Mathematische Annalen*, 97(1):737–755, 1927.

[24] P. Ramachandran, N. Parmar, A. Vaswani, I. Bello, A. Levskaya, and J. Shlens. Stand-alone self-attention in vision models. *Advances in neural information processing systems*, 32, 2019.

[25] A. Robert. *Introduction to the representation theory of compact and locally compact groups*, volume 80. Cambridge University Press, 1983.

[26] D. Romero, E. Bekkers, J. Tomczak, and M. Hoogendoorn. Attentive group equivariant convolutional networks. In *International Conference on Machine Learning*, pages 8188–8199. PMLR, 2020.

[27] D. W. Romero and J.-B. Cordonnier. Group equivariant stand-alone self-attention for vision. *ArXiv*, abs/2010.00977, 2020. URL <https://api.semanticscholar.org/CorpusID:222125298>.

[28] N. Sedaghat, M. Zolfaghari, E. Amiri, and T. Brox. Orientation-boosted voxel nets for 3d object recognition. *arXiv preprint arXiv:1604.03351*, 2016.

[29] P. Shaw, J. Uszkoreit, and A. Vaswani. Self-attention with relative position representations. In *North American Chapter of the Association for Computational Linguistics*, 2018. URL <https://api.semanticscholar.org/CorpusID:3725815>.

[30] M. Simonovsky and N. Komodakis. Dynamic edge-conditioned filters in convolutional neural networks on graphs. In *2017 IEEE Conference on Computer Vision and Pattern Recognition (CVPR)*, pages 29–38, 2017. doi: 10.1109/CVPR.2017.11.

[31] E. H. Thiede, T. S. Hy, and R. Kondor. The general theory of permutation equivariant neural networks and higher order graph variational encoders. *arXiv preprint arXiv:2004.03990*, 2020.

[32] N. Thomas, T. E. Smidt, S. M. Kearnes, L. Yang, L. Li, K. Kohlhoff, and P. F. Riley. Tensor field networks: Rotation- and translation-equivariant neural networks for 3d point clouds. *ArXiv*, abs/1802.08219, 2018. URL <https://api.semanticscholar.org/CorpusID:3457605>.

[33] A. Vaswani, N. Shazeer, N. Parmar, J. Uszkoreit, L. Jones, A. N. Gomez, Ł. Kaiser, and I. Polosukhin. Attention is all you need. *Advances in neural information processing systems*, 30, 2017.

[34] S. Villar, D. W. Hogg, K. Storey-Fisher, W. Yao, and B. Blum-Smith. Scalars are universal: Equivariant machine learning, structured like classical physics. *Advances in Neural Information Processing Systems*, 34:28848–28863, 2021.

[35] R. Wang, M. Albooyeh, and S. Ravanbakhsh. Equivariant networks for hierarchical structures. In H. Larochelle, M. Ranzato, R. Hadsell, M. Balcan, and H. Lin, editors, *Advances in Neural Information Processing Systems*, volume 33, pages 13806–13817. Curran Associates, Inc., 2020. URL https://proceedings.neurips.cc/paper_files/paper/2020/file/9efb1a59d7b58e69996cf0e32cb71098-Paper.pdf.

- [36] M. Weiler and G. Cesa. General $e(2)$ -equivariant steerable cnns. *Advances in neural information processing systems*, 32, 2019.
- [37] M. Weiler, M. Geiger, M. Welling, W. Boomsma, and T. S. Cohen. 3d steerable cnns: Learning rotationally equivariant features in volumetric data. *Advances in Neural Information Processing Systems*, 31, 2018.
- [38] E. Wigner. *Group theory: and its application to the quantum mechanics of atomic spectra*, volume 5. Elsevier, 2012.
- [39] D. E. Worrall and G. J. Brostow. Cubenet: Equivariance to 3d rotation and translation. In *European Conference on Computer Vision*, 2018. URL <https://api.semanticscholar.org/CorpusID:4795882>.
- [40] D. E. Worrall, S. J. Garbin, D. Turmukhambetov, and G. J. Brostow. Harmonic networks: Deep translation and rotation equivariance. In *Proceedings of the IEEE conference on computer vision and pattern recognition*, pages 5028–5037, 2017.
- [41] Z. Wu, S. Song, A. Khosla, F. Yu, L. Zhang, X. Tang, and J. Xiao. 3d shapenets: A deep representation for volumetric shapes. In *Proceedings of the IEEE conference on computer vision and pattern recognition*, pages 1912–1920, 2015.
- [42] R. Xu, K. Yang, K. Liu, and F. He. $e(2)$ -equivariant vision transformer. In *Uncertainty in Artificial Intelligence*, pages 2356–2366. PMLR, 2023.

A Background

A.1 Groups

Definition : A group is a non-empty set G together with a binary operation (commonly denoted by “.”, that combines any two elements a and b of G to form an element of G , denoted $a \cdot b$, such that the following three requirements, known as group axioms, are satisfied:

- *Associativity* : For all $a, b, c \in G$, one has $(a \cdot b) \cdot c = a \cdot (b \cdot c)$
- *Identity Element* : There exists an element $e \in G$ such that for every $a \in G$, one has $e \cdot a = a \cdot e = a$. Such an element is unique. It is called the *identity element* of the group.
- *Inverse* : For each $a \in G$, there exists an element $b \in G$ such that $a \cdot b = b \cdot a = e$, where e is the identity element. For each a , the element b is unique and it is called the inverse of a and is commonly denoted by a^{-1} .

Examples include set of integers \mathbb{Z} with the addition operation and the set of non-zero reals $\mathbb{R} \setminus \{0\}$ with the multiplication operation. From here on we will drop “.”, for simplicity. The group operation will be clear from the elements of the group concerned.

Group Homomorphism : Given two groups G and H , a function $\phi : G \rightarrow H$ is called a group homomorphism if $\phi(ab) = \phi(a)\phi(b)$ for any $a, b \in G$. If the map ϕ is a bijection, it is called an *isomorphism* and furthermore, if $G = H$, then an isomorphism is called *automorphism*. The set of all automorphisms of a group G with the operation of composition form a group in itself and is denoted by $\text{Aut}(G)$.

Compact Groups : A topological group is a topological space that is also a group such that the group operation and the inverse map are continuous. A compact group is a topological group whose topology realizes it as a compact topological space (see [22] for definition of topological and compact topological spaces). Some classic examples of compact groups are the groups $\text{SO}(d)$ (the group of all real orthogonal matrices in d dimensions with determinant 1), $\text{U}(d)$ (the group of all complex unitary matrices) and $\text{SU}(d)$ (the group of all complex unitary matrices with determinant 1).

Special Orthonormal Group $\text{SO}(d)$: This group comprises all real orthogonal matrices in d dimensions with a determinant of 1. These groups are associated with rotation matrices in d dimensions. Specifically, we are focused on the groups $\text{SO}(2)$ and $\text{SO}(3)$ in 2 and 3 dimensions, respectively. $\text{SO}(2)$ can be parametrized by a single angle θ , corresponding to the rotation matrix:

$$R(\theta) = \begin{bmatrix} \cos(\theta) & \sin(\theta) \\ -\sin(\theta) & \cos(\theta) \end{bmatrix}$$

Here, $R(\theta)$ signifies rotation in the x - y plane by an angle $\theta \in [0, 2\pi)$. The group $\text{SO}(3)$ can be parameterized by the so-called Euler angles. In our discussions, we adopt the z - y - z convention:

$$R_z(\alpha) = \begin{bmatrix} \cos(\alpha) & 0 & \sin(\alpha) \\ 0 & 1 & 0 \\ -\sin(\alpha) & 0 & \cos(\alpha) \end{bmatrix} \quad R_y(\beta) = \begin{bmatrix} \cos(\beta) & -\sin(\beta) & 0 \\ \sin(\beta) & \cos(\beta) & 0 \\ 0 & 0 & 1 \end{bmatrix}$$

Here, $R_z(\alpha)$ represents rotation about the z -axis by α radians, and $R_y(\beta)$ represents rotation about the y -axis by β radians. An element $R \in \text{SO}(3)$ can then be expressed as $R = R_z(\alpha)R_z(\beta)R_y(\gamma)$, where $\alpha, \gamma \in [0, 2\pi)$ and $\beta \in [0, \pi)$ are the Euler angles.

Semi-direct Product Groups : Given two groups N and H and a group homomorphism $\phi : H \rightarrow \text{Aut}(N)$, we can construct a new group $N \rtimes_{\phi} H$ defined as follows,

- The underlying set is the Cartesian product $N \times H$
- The group operation is given by $(n_1, h_1)(n_2, h_2) = (n_1\phi_{h_1}(n_2), h_1h_2)$

Special Euclidean Group $\text{SE}(d)$: The special Euclidean group $\text{SE}(d)$ encompasses all rotations and translations in d dimensions. The translation group for an d dimensional real vector is isomorphic to \mathbb{R}^n and the rotation group is given by $\text{SO}(n)$. Then, we can define a group homomorphism

$\phi : \text{SO}(d) \rightarrow \text{Aut}(\mathbb{R}^d)$, as $[\phi(R)](t) = Rt$, for any rotation $R \in \text{SO}(d)$ and a translation vector $t \in \mathbb{R}^d$. Then, the special Euclidean group $\text{SE}(d)$ is defined as $\mathbb{R}^d \rtimes_{\phi} \text{SO}(d)$. Hence the group action is given by

$$(t_1, R_1)(t_2, R_2) = (t_1 + R_1 t_2, R_1 R_2)$$

for any $(t_1, R_1), (t_2, R_2) \in \text{SE}(d)$, the identity is given by $(0, I)$, and the inverse is given by, $(t, R)^{-1} = (-R^{-1}t, R^{-1})$ for any $(t, R) \in \text{SE}(d)$.

A.2 Group Actions

Definition : If G is a group with identity element e , and X is a set, then a (left) group action α of G on X is a function $\alpha : G \times X \rightarrow X$, that satisfies the following two axioms for all $g, h \in G$ and $x \in X$:

- *Identity*: $\alpha(e, x) = x$,
- *Compatibility*: $\alpha(g, \alpha(h, x)) = \alpha(gh, x)$.

Often $\alpha(g, x)$ is shortened to $g \cdot x$. Any group G acts on itself by the group operation $g \cdot h = gh$ for any $g, h \in G$. If G acts on X , then it can also act on any function f defined on X , as $(g \cdot f)(x) = f(g^{-1} \cdot x)$.

Action of $\text{SE}(d)$: The special Euclidean group acts on a vector in \mathbb{R}^d by first applying the rotation component followed by translation. For $x \in \mathbb{R}^d$ and $(t, R) \in \text{SE}(d)$

$$(t, R) \cdot x = Rx + t,$$

gives us the action of $\text{SE}(d)$ on \mathbb{R}^d .

A.3 Group Representations

Definition : A representation of a group G is a group homomorphism ρ from G to $\text{GL}(\mathbb{C}^n)$ (group of invertible linear maps on \mathbb{C}^n), i.e,

$$\rho(g_1 g_2) = \rho(g_1) \rho(g_2) \quad \forall g_1, g_2 \in G$$

Here n is called the dimension of the representation, which can possibly be infinite. A representation is *unitary* if ρ maps to unitary linear transformation of \mathbb{C}^n .

Irreducible Representations : If we have two representations, ρ_1 and ρ_2 of dimensions n_1 and n_2 respectively, then the two can be combined by a direct sum to give another representation of dimension $n_1 + n_2$,

$$\rho_1(g) \oplus \rho_2(g) = \begin{bmatrix} \rho_1(g) & 0 \\ 0 & \rho_2(g) \end{bmatrix}.$$

A representation is said to be *completely reducible* if it can be expressed as a direct sum of other representations after maybe a change of basis, i.e,

$$U \rho(g) U^{-1} = \bigoplus_i \rho_i(g)$$

where U is a unitary change of basis matrix and the direct sum extends over some number of representations. However, for *every* group there are some representations which cannot be broken further into a direct sum of other representations. These are called the *irreducible representations* or *irreps* of the group. These irreps are the building blocks of all other representations of the group, in the sense that any representation can be written as a direct sum of the irreps:

$$\rho(g) = U \left[\bigoplus_i \rho^{(i)}(g) \right] U^{-1},$$

where again U is a change of basis matrix and $\rho^{(i)}$ are the irreps. The Peter-Weyl Theorem by [23] tells us that for a compact group G , any unitary representation ρ is completely reducible and splits into direct sum of irreducible *finite dimensional unitary representations* of G .

Irreducible Representations of $SO(2)$ and $SO(3)$: $SO(n)$ being a compact group, all its irreps are finite dimensional unitary representations. The irreps of $SO(2)$ are all of dimension one, and are indexed by the set of integers. The group $SO(2)$ can be realized by 2×2 rotation matrices, with rotation angle θ :

$$R_\theta = \begin{bmatrix} \cos \theta & \sin \theta \\ -\sin \theta & \cos \theta \end{bmatrix}.$$

With this identification of $SO(2)$, the irreducible representations of $SO(2)$ are given by,

$$\rho_k(\theta) = e^{ik\theta} \quad k \in \mathbb{Z}.$$

The irreps correspond to the Fourier basis over \mathbb{R} . The $SO(3)$ case is more involved. The irreducible representations are indexed by $\ell \in \{0, 1, 2, \dots\}$, where the ℓ 'th representation is of dimension $2\ell+1$:

$$\rho_\ell(R) = D^\ell(R) \quad \ell \in \{0, 1, 2, \dots\},$$

where D^ℓ are unitary matrices called Wigner D-matrices.

A.4 Fourier Transform

Haar Measure : There is, up to a positive multiplicative constant, a unique countably additive, nontrivial measure μ on the Borel subsets of G satisfying the following properties:

- The measure μ is left-translation-invariant: $\mu(gS) = \mu(S)$ for every $g \in G$ and all Borel sets $S \subseteq G$.
- The measure μ is finite on every compact set: $\mu(K) < \infty$ for all compact $K \subseteq G$.
- The measure μ on Borel sets $S \subseteq G$ is given by

$$\mu(S) = \inf\{\mu(U) : S \subseteq U, U \text{ open}\}.$$

- The measure μ is inner regular on open sets $U \subseteq G$:

$$\mu(U) = \sup\{\mu(K) : K \subseteq U, K \text{ compact}\}.$$

Such a measure on G is called a left Haar measure. It can be shown that as a consequence of the above properties that $\mu(U) > 0$ for every non-empty open subset $U \subseteq G$. In particular, if G is compact then $\mu(G)$ is finite and positive, so we can uniquely specify a left Haar measure on G by adding the normalization condition $\mu(G) = 1$.

Fourier Transform on Compact groups : A nice property of compact groups is that the set of (isomorphism classes of) irreducible representations of G is countable (for details see [25]). If we have a complex valued function supported on a compact group G , $f : G \rightarrow \mathbb{C}$, then the Fourier transform of f is given by

$$\hat{f}(\rho) = \frac{1}{\mu(G)} \int_G f(g) \rho(g) d\mu(G),$$

where μ is the Haar measure.

B Proof

Proof of Proposition 1. We will assume number of input channels $C = 1$. If the input is rotated and translated by $(t, R) \in \text{SO}(d)$ then input to the transformer encoder transforms as $f^{\text{in}}(\mathbf{x}, \rho) \mapsto \rho(R)f^{\text{in}}(R\mathbf{x} + t, \rho)$ and positional encoding transforms as $P(\mathbf{x}, \rho) \mapsto \rho(R)P(R\mathbf{x}, \rho)$. Let $\mathbf{q}(\mathbf{x}_i, \rho) = \mathbf{q}_i^\rho$ and similarly, \mathbf{k}_{ij} and \mathbf{v}_i . Then,

$$\begin{aligned}\mathbf{q}(\mathbf{x}_i, \rho) &\mapsto \rho(R)f^{\text{in}}(R\mathbf{x}_i + t, \rho)\mathbf{W}_Q^\rho = \rho(R)\mathbf{q}(R\mathbf{x}_i + t, \rho) \\ \mathbf{k}(\mathbf{x}_i, \mathbf{x}_j, \rho) &\mapsto \rho(R)f^{\text{in}}(R\mathbf{x}_i + t, \rho)\mathbf{W}_K^\rho + \rho(R)P(R(\mathbf{x}_i - \mathbf{x}_j), \rho) = \rho(R)\mathbf{k}(R\mathbf{x}_i + t, R\mathbf{x}_j + t, \rho) \\ \mathbf{v}(\mathbf{x}_i, \rho) &\mapsto \rho(R)f^{\text{in}}(R\mathbf{x}_i + t, \rho)\mathbf{W}_V^\rho = \rho(R)\mathbf{v}(R\mathbf{x}_i + t, \rho)\end{aligned}$$

Let $s(\mathbf{x}_i, \mathbf{x}_j, \rho) = s_{ij}^\rho$ and $\alpha(\mathbf{x}_i, \mathbf{x}_j, \rho) = \alpha_{ij}^\rho$. Then using the fact $\rho(R)$ is unitary we have,

$$\begin{aligned}s(\mathbf{x}_i, \mathbf{x}_j, \rho) &= \sum_{\rho, \rho'} w_{\rho, \rho'}^{(1)} \frac{\mathbf{q}(\mathbf{x}_i, \rho)^\dagger \mathbf{k}(\mathbf{x}_i, \mathbf{x}_j, \rho')}{\sqrt{d_k}} \\ &\mapsto \sum_{\rho, \rho'} w_{\rho, \rho'}^{(1)} \frac{\mathbf{q}(R\mathbf{x}_i + t, \rho') \rho(R)^\dagger \rho(R)' \mathbf{k}(R\mathbf{x}_i + t, \mathbf{x}_j, \rho')}{\sqrt{d_k}} \\ &= \sum_{\rho, \rho'} w_{\rho, \rho'}^{(1)} \frac{\mathbf{q}(R\mathbf{x}_i + t, \rho) \mathbf{k}(R\mathbf{x}_i + t, \mathbf{x}_j, \rho')}{\sqrt{d_k}} \\ &= \sum_{\rho, \rho'} w_{\rho, \rho'}^{(1)} s(R\mathbf{x}_i + t, R\mathbf{x}_j + t, \rho') \\ &= s(R\mathbf{x}_i + t, R\mathbf{x}_j + t, \rho)\end{aligned}$$

The first equality follows from the fact that since $C = 1$ the *vec* operation is no longer needed. Since α is obtained by taking the softmax of s , it follows that.

$$\alpha(\mathbf{x}_i, \mathbf{x}_j, \rho) \mapsto \alpha(R\mathbf{x}_i + t, R\mathbf{x}_j + t, \rho).$$

Finally,

$$\begin{aligned}f^{\text{out}}(\mathbf{x}_i, \rho) &\mapsto \sum_{\rho, \rho'} \sum_j w_{\rho, \rho'}^{(2)} \alpha(R\mathbf{x}_i + t, R\mathbf{x}_j + t, \rho') \rho(R) \mathbf{v}(R\mathbf{x}_j + t, \rho') \\ &= \rho(R) \left(\sum_{\rho, \rho'} \sum_j w_{\rho, \rho'}^{(2)} \alpha(R\mathbf{x}_i + t, R\mathbf{x}_j + t, \rho') \mathbf{v}(R\mathbf{x}_j + t, \rho') \right) \\ &= \rho(R) f^{\text{out}}(R\mathbf{x}_i + t, \rho)\end{aligned}$$

□

C Experiment Details

Here we provide the details of all the experiments we have conducted. Table 4 shows detailed results on the two datasets.

Datasets	Model	Radial Resolution	Frequency Cutoff	Accuracy	Parameter ($\sim \times 10^6$)
Rotated MNIST	Steerable Convolution	$r = 2$	$k = 4$	98.69 ± 0.05	1.00
			$k = 8$	98.93 ± 0.02	1.98
		$r = 4$	$k = 4$	98.72 ± 0.02	1.98
			$k = 8$	98.97 ± 0.01	3.94
	Steerable Convolution (Without Transformer)	$r = 2$	$k = 4$	98.59 ± 0.08	0.24
			$k = 8$	98.92 ± 0.04	0.47
		$r = 4$	$k = 4$	98.70 ± 0.05	0.47
			$k = 8$	98.97 ± 0.05	0.92
	Steerable Transformer	$r = 2$	$k = 4$	98.78 ± 0.08	0.91
			$k = 8$	99.03 ± 0.04	1.78
		$r = 4$	$k = 4$	98.82 ± 0.04	1.13
			$k = 8$	99.03 ± 0.06	2.24
ModelNet10 (z Rotation) (SO(3) Rotation)	Steerable Convolution	$r = 1$	$\ell = 4$	89.40 ± 0.53	0.90
				86.78 ± 0.62	
		$r = 2$	$\ell = 4$	90.13 ± 0.52	1.08
				86.62 ± 0.25	
	Steerable Convolution (Without Transformer)	$r = 1$	$\ell = 4$	89.08 ± 0.91	0.34
				86.19 ± 0.55	
		$r = 2$	$\ell = 4$	89.51 ± 0.55	0.48
				86.58 ± 0.92	
	Steerable Transformer	$r = 1$	$\ell = 4$	89.52 ± 0.55	0.90
				85.87 ± 0.74	
		$r = 2$	$\ell = 4$	90.40 ± 0.25	0.92
				86.80 ± 0.58	

Table 4: Comparison of Steerable convolution and steerable transformers. The mean and sd are provided for 5 separate runs

C.1 Rotated MNIST

For this experiment we have used $w_{\rho\rho'}^{(1)}$ as learnable scalars which are same for all ρ and $w_{\rho\rho'}^{(2)} = \mathbb{1}_{\rho=\rho'}$. Using these weights the steerable attention mechanism boils down to:

$$s_{ij} = \sum_{\rho'} w_{\rho'}^{(1)} s(\mathbf{q}_i^{\rho'}, \mathbf{k}_{ij}^{\rho'}) \quad \alpha_{ij} = \frac{\exp(|s_{ij}|)}{\sum_{j'=1}^N |s_{ij'}|} \quad f^{\text{out}}(\mathbf{x}_i, \rho) = \sum_{j=1}^N \alpha_{ij} \mathbf{v}_j^{\rho}$$

The network architecture is shown in Figure 4. The networks are trained using Adam Optimizer [15] with an initial learning rate of $5e-3$ which steps down by a factor of 0.5 every 20 epochs and weight decay of $5e-4$, for 150 epochs. The angular resolution for the steerable convolution layers (denoted by the parameter *angle* in Figure 4) is fixed at 40. More detailed experiments where we have varied the radial resolution (r) and the frequency cutoff (*maxm*) are presented in Table 4. We used a batch size of 100 and it took 2.5 hrs to train our largest model on four 16GB GPUs.

C.2 ModelNet10

The point cloud data with 2048 point can be found here. For this experiment with z rotation we have used the most general model where both $w_{\rho\rho'}^{(1)}$ and $w_{\rho\rho'}^{(2)}$ are learnable scalars. For the SO(3) rotation we used the same scalar choice as Rotated MNIST. The network architecture is shown in Figure 5. The networks are trained using Adam Optimizer [15] with an initial learning rate of $1e-3$ which steps down by a factor of 0.5 every 20 epochs, for 50 epochs. The angular resolution for

```

 $SE2ConvType1(1, 24, 5, r, angle, maxk),$ 
 $CGNonLinearity2D(),$ 
 $SE2ConvType2(24, 48, 5, r, angle, maxk),$ 
 $SteerableBatchNorm2D(),$ 
 $AvgPool2D(2),$ 
 $SE2TransformerEncoder(18, 5, maxk, layers = 1),$ 
 $SE2ConvType2(48, 48, 5, r, angle, maxk),$ 
 $CGNonLinearity2D(),$ 
 $SE2ConvType2(48, 96, 5, r, angle, maxk),$ 
 $SteerableBatchNorm2D(),$ 
 $AvgPool2D(2),$ 
 $SE2TransformerEncoder(96, 4, maxk, layers = 1),$ 
 $SE2ConvType2(96, 64, 7, r, angle, maxk),$ 
 $NormFlatten(),$ 
 $Linear(144, 128),$ 
 $BatchNorm1d(128),$ 
 $ReLU(),$ 
 $Dropout(0.7),$ 
 $Linear(128, 10)$ 

```

(a) Steerable Transformer

```

 $SE2ConvType1(1, 24, 5, r, angle, maxk),$ 
 $CGNonLinearity2D(),$ 
 $SE2ConvType2(24, 48, 5, r, angle, maxk),$ 
 $SteerableBatchNorm2D(),$ 
 $AvgPool2D(2),$ 
 $SE2ConvType2(48, 96, 5, r, angle, maxk),$ 
 $CGNonLinearity2D(),$ 
 $SE2ConvType2(96, 192, 5, r, angle, maxk),$ 
 $SteerableBatchNorm2D(),$ 
 $AvgPool2D(2),$ 
 $SE2ConvType2(192, 192, 7, r, angle, maxk),$ 
 $NormFlatten(),$ 
 $Linear(192, 128),$ 
 $BatchNorm1d(128),$ 
 $ReLU(),$ 
 $Dropout(0.7),$ 
 $Linear(128, 10)$ 

```

(b) Steerable Convolution

Figure 4: ModelNet10 Architecture

the steerable convolution layers (denoted by the parameter $angle$ in Figure 5) is fixed at 40. More detailed experiments where we have varied the radial resolution (r) and the frequency cutoff ($maxl$) are presented in Table 4. We used a batch size of 5 and it took 12 hrs to train our largest model on one 16GB GPU.

```

 $SE3ConvType1(1, 9, 5, r, angle, maxl),$ 
 $CGNonLinearity3D(),$ 
 $SE3ConvType2(9, 18, 3, r, angle, maxl),$ 
 $SteerableBatchNorm3D(),$ 
 $AvgPool3D(4),$ 
 $SE3TransformerEncoder(18, 3, maxl, n\_layers = 1),$ 
 $SE3ConvType2(18, 36, 3, r, angle, maxl),$ 
 $CGNonLinearity3D(),$ 
 $SE3ConvType2(36, 72, 3, r, angle, maxl),$ 
 $SteerableBatchNorm3D(),$ 
 $AvgPool3D(4),$ 
 $SE3TransformerEncoder(72, 4, maxl, n\_layers = 1),$ 
 $SE3ConvType2(72, 144, 2, r, angle, maxl),$ 
 $NormFlatten(),$ 
 $Linear(144, 128),$ 
 $BatchNorm1d(128),$ 
 $ReLU(),$ 
 $Dropout(0.7),$ 
 $Linear(128, 10)$ 

```

(a) Steerable Transformer

```

 $SE3ConvType1(1, 9, 5, r, angle, maxl),$ 
 $CGNonLinearity3D(),$ 
 $SE3ConvType2(9, 36, 3, r, angle, maxl),$ 
 $SteerableBatchNorm3D(),$ 
 $AvgPool3D(4),$ 
 $SE3ConvType2(36, 72, 3, r, angle, maxl),$ 
 $CGNonLinearity3D(),$ 
 $SE3ConvType2(72, 72, 3, r, angle, maxl),$ 
 $SteerableBatchNorm3D(),$ 
 $AvgPool3D(4),$ 
 $SE3ConvType2(72, 144, 2, r, angle, maxl),$ 
 $NormFlatten(),$ 
 $Linear(144, 128),$ 
 $BatchNorm1d(128),$ 
 $ReLU(),$ 
 $Dropout(0.7),$ 
 $Linear(128, 10)$ 

```

(b) Steerable Convolution

Figure 5: ModelNet10 Architecture